Obtaining Three-dimensional Information From Forests using Polarimetric Interferometry

Stephen McNeill, David Pairman
Landcare Research New Zealand,
Box 69, Lincoln, New Zealand.
mcneills@landcareresearch.co.nz

Abstract

In this paper we describe the principles of polarimetric radar interferometry (polinsar). This new mode of radar imaging provides three-dimensional information on the thickness of the forestry layer by gathering full-polarisation imagery at either end of a coherent interferometer, and solving an interferometric coherence maximisation problem, yielding the dominant scattering modes and fixing the effective scattering centres for these modes. When several effective scattering centres are isolated the interferometric phase difference is related to the height difference between the top of the forest canopy and the ground.

We demonstrate successful inversion of the polinsar polarisation-coherence relations, using test data of Baikal, Russia, from the 1994 SIR-C mission. The solution process was made more complicated by the non-reciprocal nature of the SIR-C test data. The forest height estimates are numerically sensitive to the precise implementation of the inversion methodology. Despite the numerical complexity, polinsar yields information that is difficult to achieve by other means.

Keywords: remote sensing, radar, SAR, polarimetry, interferometry, polinsar

1 Introduction

Polarimetric interferometry (known as *polinsar*) has become a popular area for research since the late 1990s, after its description by Cloude and Papathanassiou [1]. It is an extension of conventional interferometry where full-polarisation information is gathered at either end of the interferometric baseline. The method is most usefully applied to targets that exhibit volume scattering, such as forests, where the results from conventional interferometry become ambiguous.

While conventional interferometry generates a scalar measure of scatterer phasing, known as coherence, polinsar generates a complex matrix measure of coherence, containing both polarimetric and interferometric components. The polinsar coherence matrix represents new information, and this can be processed to generate details of the vertical distribution of scatterers within the resolution cell. Essentially, polinsar allows for a limited amount of three-dimensional discrimination in the volume scattering resolution cell.

This paper describes an experiment to reproduce the basic result of polarimetric interferometry, using repeat-pass full-polarimetric imagery from the NASA Shuttle Imaging Radar C mission of October 1994. The motivation of the work was to develop a basic capability to process this new form of imaging arrangement, and to assess its potential for the New Zealand environment.

Section 2 of this paper describes the characteristics of the polarimetric interferometry system. Section 3 describes the test sites and data, and the processing methodology used in the experiment. Finally, section 4 gives some preliminary results from the experiment. As results are preliminary, the final version of this paper will give a quantitative account of the observed interactions.

2 PolInSAR Imaging

2.1 The Measurement System

The electromagnetic wave state is defined by the amplitude, phase, orientation and ellipticity [2], and by making several straightforward physical assumptions [3], it is possible to show that the radar backscatter response of the target (see figure 1) can be calculated as follows:

$$\sigma_n(\psi_r, \chi_r, \psi_t, \chi_t) = 4\pi \left| \vec{p}_r S \, \vec{p}_t \right| \quad (1)$$

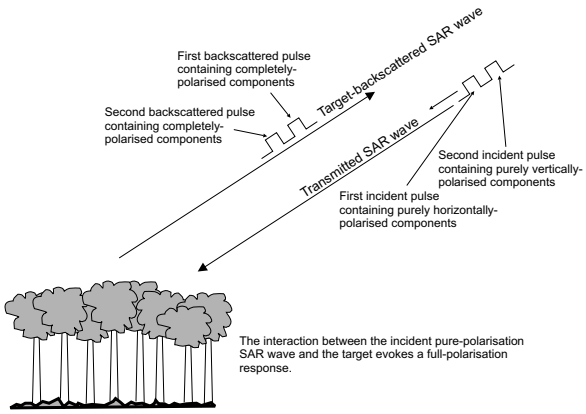

Figure 1: The full-polarisation imaging system

In equation 1, which defines the *polarisation synthesis* process [4], σ_{rt} is the target backscatter, ψ and χ are the orientation and ellipticity respectively, the subscripts "r" and "t" refer to the "received" and "transmitted" components of ψ and χ, the vector $\vec{p}$ refers to the field polarisation vector, and S is the complex 2x2 scattering matrix.

Versions of the polarisation synthesis equation 1 above also exist that are defined in terms of unitary transformations of the scattering matrix S. One, in particular, is the 3x3 complex Hermitian coherency matrix T [5]. Figure 1 and the associated polarisation synthesis equation 1 describe polarimetric imaging.

In interferometry, two radar transmitters spaced a short distance apart [6] are arranged as shown in figure 2. The distance between the two radar positions is on the order of metres (airborne) to, perhaps, a kilometre or so (satellite), depending on the geometry of the imaging arrangement [7]. The two images are taken at the same time from the same platform (*simultaneous interferometry*), or the target may be over-flown on two separate runs (*repeat-pass interferometry*).

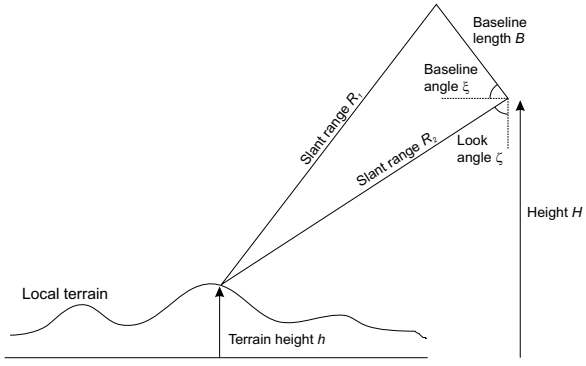

Figure 2: Geometry of interferogram-generation

Conventional interferometry uses the imaging arrangement as in figure 2 above, with a single-polarisation common to both transmitter and receiver.

By contrast, in *polarimetric* interferometry, the same physical arrangement in figure 2 is used, however the full-polarisation matrix is gathered, as outlined in figure 1.

The polarimetric interferometric process generates the outer product of the polarimetric information at either end of the interferometer, analogous to the complex product of two complex scalars in conventional interferometry. This process generates a 6x6 Hermitian positive semi-definite matrix T_6 [1,8]:

$$T_6 = \begin{bmatrix} [T_{11}] & [\Omega_{12}] \\ [\Omega_{12}]^{*T} & [T_{22}] \end{bmatrix} \quad (2)$$

In equation 2, $[T_{11}]$ and $[T_{22}]$ are Hermitian coherency matrices, representing the full polarimetric information for the images at the ends of the interferometric baseline. The $[\Omega_{12}]$ term contains new information, representing a combination of phase and polarisation information that exists *between* the two images. In conventional interferometry, the phase information is a scalar. It can be shown [1] that $[\Omega_{12}]$ adds new information to the imaging system.

2.2 PolInSAR Coherence

In conventional interferometry, the coherence γ (with $\gamma \in [0,1]$) is the magnitude of the scalar product of the complex signal from the two ends of the interferometer. When γ has a value of 0, scatterers have no phase correspondence, and are effectively incoherent. When γ has a value of 1, the scatterers have perfect correspondence, and are completely coherent. For conventional interferometry, the local estimate $\hat{\gamma}$ of coherence γ between the two images s_1 and s_2, at any given location in the interferogram is defined as follows:

$$\hat{\gamma} = \frac{\sum s_1 s_2^*}{\sqrt{\sum s_1 s_1^* \sum s_2 s_2^*}} \quad (3)$$

In equation 3, s^* represents the complex conjugate of s and the summation is taken over a small region in the image. Defined in this manner, $\hat{\gamma}$ is a biased estimator [9], but provided care is taken in its interpretation, it is a reliable indicator of the phase coherence of the scatterers. Conventionally, coherence is used in conventional interferometry as a quality measure, since areas of low coherence correspond to regions where the interferogram is of poor quality.

In polinsar, there is a generalised version of coherence defined thus [1]:

$$\gamma = \frac{\left|\left\langle \underline{w}_1^{*T} [\Omega_{12}] \underline{w}_2 \right\rangle\right|}{\sqrt{\left\langle \underline{w}_1^{*T} [T_{11}] \underline{w}_1 \right\rangle \left\langle \underline{w}_2^{*T} [T_{22}] \underline{w}_2 \right\rangle}} \quad (4)$$

In equation 4, $\underline{w}_1$ and $\underline{w}_2$ are normalised complex vectors that represent the scattering mechanisms, defined in terms of the scattering matrices from each end of the interferometer [1]. Equation 4 makes it clear that polinsar coherence depends on the particular polarimetric scattering mechanism chosen, and it is reasonable to ask which particular choice of scattering mechanisms $\underline{w}_1$ and $\underline{w}_2$ will result in the highest coherence γ.

2.3 Polinsar Coherence Interpretation

It can be shown [1] that the optimum solution that maximises the coherence in equation 4 can be written as the solution to two eigenvalue problems with common eigenvalues $\nu = \lambda_1 \lambda_2^*$.

$$\begin{aligned} [T_{11}]^{-1} [\Omega_{12}]^{*T} [T_{22}]^{-1} [\Omega_{12}] \underline{w}_1 &= \nu \underline{w}_1 \\ [T_{22}]^{-1} [\Omega_{12}]^{*T} [T_{11}]^{-1} [\Omega_{12}] \underline{w}_2 &= \nu \underline{w}_2 \end{aligned} \quad (5)$$

The solution to equation 5 gives three values ν_j, with $\nu_1 \geq \nu_2 \geq \nu_3 \geq 0$, each with a related vector representing the optimum scattering mode. The optimum scattering modes can be physically interpreted as having statistical independence between the scattering mechanisms. Moreover, the phase difference between the interferograms formed from these optimum scattering modes represents the difference in phase between the effective phase centres of the corresponding scattering mechanisms. The interferograms formed in this way will have the most accurate estimate of the phase difference between them, since the coherence has been optimised.

For targets where there is only one dominant scattering mechanism, there is only one scattering phase centre, and the topographic phase from this interferogram fixes the effective scattering centre. For targets where there is a vertical distribution of scatterers, and where there are three independent scattering mechanisms, as one might expect in a forest, the phase difference between the interferograms represents the topographic phase difference (i.e. the height difference) between the phase centres that are represented by each scattering mechanism. Thus, provided one can identify the relationship between the phase centre and the physical target, by way of a physical or mathematical model, one can deduce the height difference of the layers in the vertically-distributed scatterer, such as canopy thickness or forest height. While this is not true three-dimensional imaging in the strictest sense, the procedure does yield true three-dimensional information.

3 Experimental Method

3.1 Test Site

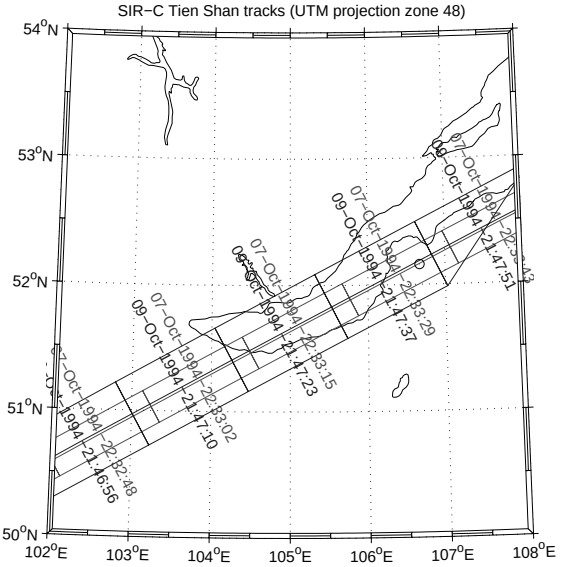

Figure 3: SIR-C tracks covering the test site, with the nominal test site location marked

Polinsar is of interest to Landcare Research New Zealand, and other researchers, since it potentially provides information on forest and canopy height, which are difficult and time-consuming to measure over extensive areas of forest [10]. However, it is not clear how successful repeat-pass polinsar would be in the New Zealand environment, where the interferometric coherence decays quickly because of temporal change.

Full-polarisation repeat-pass satellite imagery suitable for polinsar is available for a few selected days from the Shuttle Imaging Radar C (SIR-C) mission, which flew in April and October 1994 [11]. SIR-C was a joint project of NASA, the German Space Agency (DARA) and the Italian Space Agency (ASI). The antenna structure consisted of three individual antennas, operating at L-band (24 cm wavelength), C-band (5.8 cm wavelength) and X-band (3 cm wavelength). The L- and C-band antennas were constructed in the form of separate planar arrays so that they were able to transmit and receive both horizontal and vertical polarisation, and, for certain operating periods, were able to generate full-polarisation imagery.

None of the SIR-C images gathered over New Zealand is suitable for polinsar, but there are dozens of images from other parts of the world that are suitable for testing polinsar algorithms, and these are datasets widely used within the polinsar research community. In the present study, the data used consists of two SIR-C L-band single-look complex

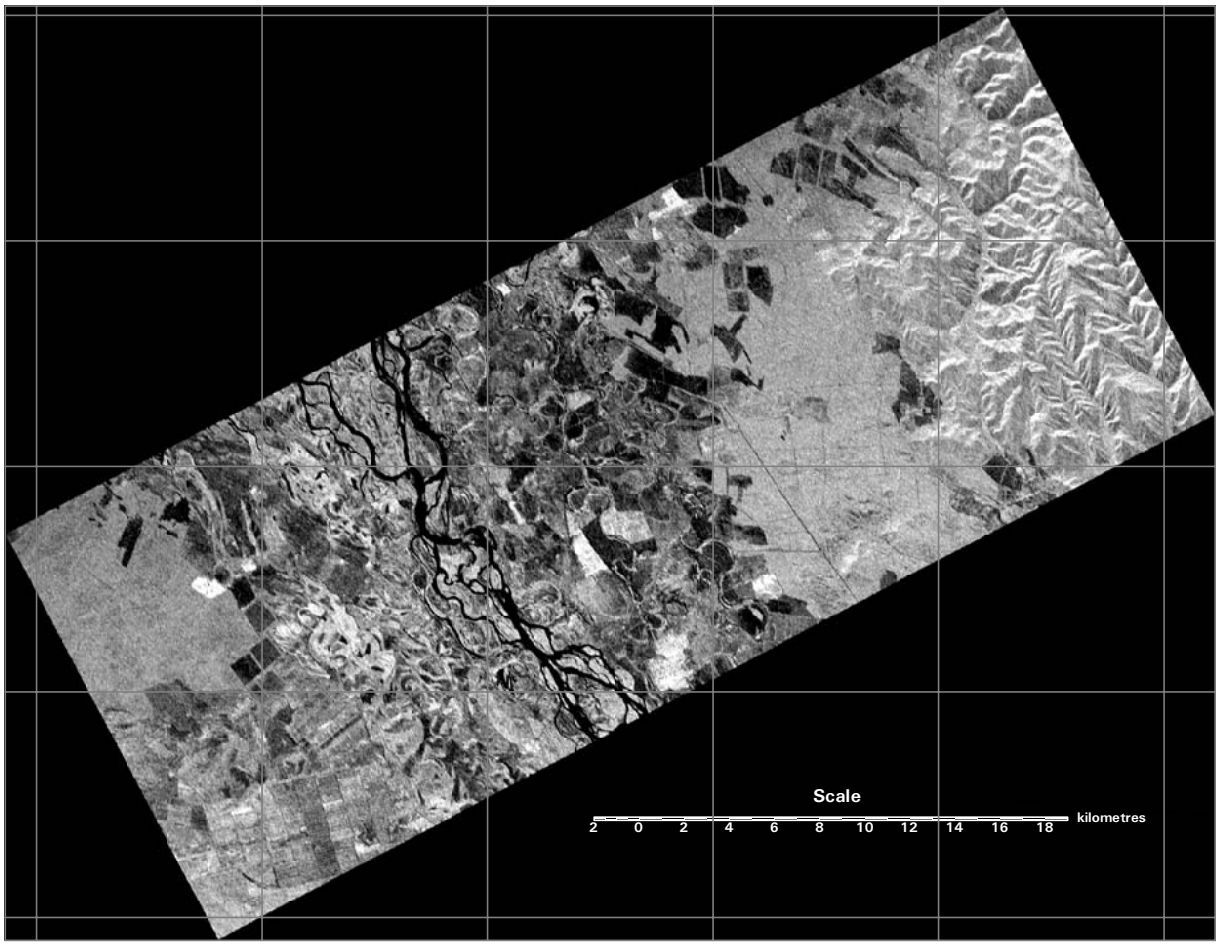

Figure 4: Geocoded SIR-C L-band total power image of the Baikal test site

image pairs of the Tien Shan test site. Although this test site is in China, part of the acquired SIR-C orbital track covers an area to the south and east of Lake Baikal, Buriatia, Russia. The nominal test site location is latitude 52.16º North, 106.67º East, shown in map form in figure 3.

3.2 Supplied Data

In order for polinsar to be successfully applied, single-look complex (SLC), full scattering matrix imagery is required. For SIR-C, this is supplied in a custom format, in scattering matrix form [3].

Reciprocity of the scattering matrix is normally enforced in full-polarisation systems, ensuring that the cross-polarisation terms S_{hv} and S_{vh} are equal, but this is not so in the case of SIR-C SLC data. Residual phase differences between S_{hv} and S_{vh} are therefore likely because of phase differences between the horizontal and vertical system chains, and mis-calibrations within the antenna system [12].

Rigorous phase calibration requires ground truth targets of known amplitude and phase characteristics, which were not available in this case. Therefore, a simplified phase calibration method was used, that assumed that the non-reciprocal scattering matrix was solely due to simple phase differences between the horizontal and vertical system chains [13]. It was also assumed that the cross talk between the horizontal and vertical channels was negligible. Published results from the literature [12] suggest that these are reasonable assumptions.

The resultant image, after phase calibration, is a reciprocal scattering matrix, from which the coherency matrix T can be generated for polinsar processing. A multi-looked, geocoded version of the L-band total power P_T, generated from the calibrated scattering matrix, where $P_T = \sigma^2_{HH} + 2\sigma^2_{HV} + \sigma^2_{VV}$, is shown in figure 4.

3.3 Polinsar Processing

In polinsar, we eventually reach an eigenvalue problem that yields three optimal coherence values $\tilde{\gamma}_1$, $\tilde{\gamma}_2$, and $\tilde{\gamma}_3$, where:

$$\begin{bmatrix} \tilde{\gamma}_1 \\ \tilde{\gamma}_2 \\ \tilde{\gamma}_3 \end{bmatrix} = \text{function}\left(\begin{bmatrix} \text{local height} \\ \text{extinction} \\ \text{vegetation height} \end{bmatrix} \right) \quad (6)$$

The variables on the right-hand-side of the equation are examples of those required for a particular

coherence-vegetation model. This can be interpreted as saying that the optimal coherence values are a function of certain vegetation and topography parameters. Normally, however, we are interested in recovering the vegetation and/or topography parameters. Thus, we wish to invert this coherence-vegetation relationship to estimate:

$$\begin{bmatrix} \text{local height} \\ \text{extinction} \\ \text{vegetation height} \end{bmatrix} = \text{function}^{-1}\left(\begin{bmatrix} \tilde{\gamma}_1 \\ \tilde{\gamma}_2 \\ \tilde{\gamma}_3 \end{bmatrix} \right) \quad (7)$$

Equation 7 illustrates that we require a function that yields vegetation and topography parameters, given the optimal coherence values. Equation 7 is straightforward to describe, but there are no closed form solutions to a comprehensive radar-forest model [1,8,14], so numerical solutions must instead be developed.

A key point to understand is that the absolute phase difference between the interferograms generated from the optimal-coherence problem, as outlined in section 3, does not necessarily correspond to the height difference between the forest canopy top and the ground level. The absolute phase difference yields a height that is significantly less than the true forest height [14]. Therefore, the absolute phase difference must be converted to true height difference by using an appropriate model that relates phase difference to distance through the forest canopy.

In the present research, we followed an approach recently developed by Cloude and Papathanassiou [8,14], which involves an iterative solution of a non-linear optimisation problem, based on a two-layer model of the vegetated land surface. Although this is a very simple model, it is supported by experiments from polarimetric tomography [15], which have established the basic scattering modes within the forest layer. However, we note that the development of suitable models for polinsar, and their efficient numerical solution is the subject of considerable ongoing research.

4 Results

The phase calibration procedure was tested by estimating the polarimetric phase in known areas of forestry and low-stature vegetation. The result was compared with the expected polarisation phase behaviour from similar kinds of forestry and vegetation in New Zealand, and found to agree. Although this is a qualitative comparison, with no available ground truth it was the only practical option.

At the time of writing, the numerical results from the polinsar coherence-inversion model, outlined above in section 3, are still undergoing some refinement. The final paper and presentation will show quantitative model results.

5 Discussion

Processing of the Baikal L-band SIR-C data to generate three-dimensional information of the forest was difficult, for several reasons. First, there is no ground-truth, making it necessary to make “educated guesses” concerning the nature of some of the targets in the scene. Second, the SIR-C single-look complex data come in non-reciprocal form, so that the horizontal and vertical channels are not necessarily orthogonal, introducing some significant complications into the processing chain. Finally, the numerical inversion of the polarimetric-coherence model is complicated, since a six-variable optimisation is required with relatively noisy data, necessitating the development of a robust implementation of the inversion methodology.

5.1 Polinsar in New Zealand

Although there is, at present, no suitable full-polarisation data for polinsar processing in New Zealand, it is possible that this method of processing will be feasible in the future, once data from the L-band ALOS PALSAR [16] and Radarsat-2 [17] platforms is available. Unfortunately, the full-polarisation mode of ALOS PALSAR will only be available for limited periods of time, limiting the number of opportunities for suitable data acquisition. Radarsat-2 will support a calibrated full-polarisation mode, but uses a relatively short wavelength (5.6 cm) and a relatively long repeat interval (24 days), so that it is not yet certain how successful this mode will be in New Zealand.

In the near future, the research in Landcare Research is directed towards the development of suitable models of vegetation for New Zealand conditions, and several key experiments to characterise the temporal coherence of forestry targets.

6 Conclusions

Polarimetric radar interferometry (polinsar) provides a way to generate three-dimensional information on the thickness of the forestry layer. It achieves this by gathering full-polarisation imagery at either end of a coherent interferometer, and solving a coherence maximisation problem, yielding the dominant scattering modes that fix the effective scattering centres for the modes. When several effective scattering centres can be isolated, as in a forest layer, the interferometric phase difference can be related to the height difference between the top of the forest canopy and the ground.

We have demonstrated inversion of the polarisation coherence relations. We have found the solution to be somewhat complicated by the non-reciprocal nature of the SIR-C test data, and numerically sensitive to the precise implementation of the inversion methodology. However, the solution produces information that is

difficult to achieve by other means in remote sensing, giving promise of useful information for forestry, ecology and conservation efforts in this country.

7 Acknowledgements

This work was funded by the Foundation for Research, Science and Technology.

8 References

[1] Cloude, S.R. Papathanassiou, K.P "Polarimetric SAR interferometry", *IEEE Transactions on Geoscience and Remote Sensing*, 36:1551–1565 (1998).

[2] Inan, U.S., Inan, A.S., Engineering electromagnetics, Addison Wesley Longman. 804 p (1999).

[3] Ulaby, F.T. van Zyl, J.J. "Wave properties and polarization". In: Ulaby, F.T. Elachi, C. (eds.) Radar polarimetry for geoscience applications. Norwood, Ma, Artech House, pp 1–16 (1990).

[4] van Zyl, J.J. Zebker, H.A. Elachi, C. "Imaging radar polarization signatures: theory and observation". Radio Science. 22:529–543 (1987).

[5] Cloude, S.R. Pottier, E. "A review of target decomposition theorems in radar polarimetry", IEEE Transactions on Geoscience and Remote Sensing, 34:498–518 (1996).

[6] Graham, L.C. "Synthetic interferometer radar for topographic mapping", *Proceedings IEEE*, 62:763–768 (1974)

[7] Madsen, S.N. Zebker, H.A. "Imaging radar interferometry". In: Henderson, F.M. Lewis, A.J. (eds.) *Principles & applications of imaging radar*, New York, USA. J Wiley. pp. 359–380 (1998).

[8] Papathanassiou, K.P. Cloude, S.R. "Single-baseline polarimetric SAR interferometry", *IEEE Transactions on Geoscience and Remote Sensing*, 39:2352–2363 (2001).

[9] Touzi, R. Lopes, A. Bruniquel, J. Vachon, P.W. "Coherence estimation for SAR imagery", *IEEE Trans. Geoscience and Remote Sensing*, 37(1), pp 135–149.

[10] McNeill, S.J. Pairman, D. "*Polarimetric interferometry: prospects for vegetation modelling in New Zealand"*, Landcare Research New Zealand Ltd Research Report LC0203/020, 33 p (2002).

[10] Jordan, R.L. Huneycutt, B.L. Werner, M. "The SIR-C/X-SAR synthetic aperture radar system", *IEEE Transactions on Geoscience and Remote Sensing*, 33:829–839 (1995).

[11] Evans, D.L. Plaut, J.J. Stofan, E.R. "Overview of the spaceborne imaging radar-C/X-band synthetic aperture radar (SIR-C/X-SAR) missions", *Remote Sensing of the Environment, 59:*135–140 (1997).

[12] Freeman, A. Alves, M. Chapman, B. Cruz, J. Kim, Y. Shaffer, S. Sun, J. Turner, E. Sarabandi, K. "SIR-C data quality and calibration results", *IEEE Trans. Geoscience and Remote Sensing*, 33(4), pp 848–857 (1995).

[13] Zebker, H.A. van Zyl, J.J. Elachi, C. "Polarimetric radar system design", In: Ulaby, F.T. Elachi, C. (eds.) Radar polarimetry for geoscience applications. Norwood, Ma, Artech House, pp 273–313 (1990).

[14] Cloude, S.R. Papathanassiou, K.P. "Three-stage inversion process for polarimetric SAR interferometry", *IEE Proc. Radar Sonar Navigation*, 150(3) (2003).

[15] Reigber, A. Moreira, A. "First demonstration of airborne SAR tomography using multi-baseline L-band data", *IEEE Trans. Geoscience and Remote Sensing*, 38(5), pp 2142–2152 (2000).

[16] Kimura, H. Itoh, N. "ALOS PALSAR: The Japanese second-generation spaceborne SAR and its application", *Proceedings Society of Photo-optical Instrumentation Engineers (SPIE),* 4152:110–119 (2000).

[17] Brûlé, L. Baeggli, H. "*RADARSAT-2 program update"*, CD-ROM Proceedings, International Geoscience and Remote Sensing Symposium (IGARSS-02), Toronto, Canada (2002).